PCCP

Accepted Manuscript

ROYAL SOCIETY OF CHEMISTRY

www.rsc.org/pccp

Journal Name

RSCPublishing

ARTICLE

Practical approach to calculate time evolutions of magnetic field effects on photochemical reactions in nano-structured materials

Cite this: DOI: 10.1039/x0xx00000x

Received 00th January 2012,
Accepted 00th January 2012

DOI: 10.1039/x0xx00000x

www.rsc.org/

Tomoaki Yago*[a] and Masanobu Wakasa[a]

Practical method to calculate time evolutions of magnetic field effects (MFEs) on photochemical reactions involving radical pairs is developed on the basis of the theory of the chemically induced dynamic spin polarization proposed by Pedersen and Freed. In the theory, stochastic Liouville equation (SLE) including the spin Hamiltonian, diffusion motions of the radical pair, chemical reactions, and spin relaxations are solved by using the Laplace transformation technique. In our practical approach, time evolutions of the MFEs are successfully calculated by applying Miller-Guy method instead of the final value theorem to the inverse Laplace transformation process. Especially, the SLE calculations are completed in a short time when the radical pair dynamics can be described by the chemical kinetics consisting of diffusions, reactions and spin relaxations. The SLE analysis with the short calculation time enables one to examine the various parameter sets for fitting the experimental date. Our study demonstrates that simultaneous fitting of the time evolution of the MFE and of the magnetic field dependence of the MFE provides valuable information on the diffusion motions of the radical pairs in nano-structured materials such as micelles where the lifetimes of radical pairs are longer than hundred nano-seconds and the magnetic field dependence of the spin relaxations play major role for the generation of the MFE.

Introduction

Magnetic field effects (MFEs) on photochemical reactions through radical pairs (RPs) and biradicals have attracted the considerable attentions since the reproducible observations of the MFE phenomena supported by the solid theory in the middle of 1970s.[1–3] An unique aspect of the MFE is that the magnetic energy, which is smaller than the thermal energy, can alter the rate of the RP recombination reactions that proceed via the activated states. According to the Pauli exclusion principle, the singlet RP can react to form the recombination product whereas the triplet RP have no reactivity. Magnetic field can change the populations of the singlet and the triplet RPs therefore affects the recombination reaction of RP, quantum mechanically. The changes of the populations of the singlet and triplet RPs occur in nanometer-separated RP where the singlet-triplet energy splitting in RP is comparable with or less than the magnetic interactions in RP such as the hyperfine coupling constants and the *g*-value differences (Δg) between radicals. In contrast, the recombination reactions efficiently proceed in the contact RP. Thus the MFEs are generated when the radicals diffuse back and forth between the nanometer-separated and the contact RPs. Consequently the diffusion motions of the radicals in the nanometer space significantly influence the MFEs on the RP. It has been proposed that the molecular diffusion process in nanometer space can be probed from the observation of the MFEs on RPs.[4–7]

In the nano-structured materials, the diffusion motions of molecules are often controversial to understand the mechanisms of the chemical reactions because of their heterogeneous characters. On the other hand, the large and clear MFEs have been observed in the photochemical reactions systems where the RPs are confined in the nanometer-structured materials such as micelles[8–10] and mesoporous silicates.[11,12] Therefore MFE study can be a powerful tool to probe the heterogeneous molecular diffusions in nano-structured materials. Recently we discussed the solute molecular diffusions in mesoporous silicates of MCM-41[8] and in ionic liquids[13–19] from the observations of the MFEs on the photochemical reactions. To discuss the solute molecular diffusions, the observed magnetic field dependences (*B*-curve) of the yield of the radicals were fitted by using the stochastic Liouville equation (SLE)[20,21] in which the spin dynamics, diffusive and reactive dynamics were treated simultaneously. The procedure of our SLE analysis followed the SLE analysis reported by Pedersen and Freed.[22–24]

First, the time (t)-domain differential equation is Laplace transformed to the frequency domain algebraic equations. Then the frequency domain algebraic equation is numerically solved with the matrix equation. Finally, the obtained result is recovered by the inverse Laplace transformation. In the final step, the final value theorem is employed to obtain the limiting values ($t \rightarrow \infty$) of the density matrix. The use of the final value theorem greatly reduces the calculation procedure and time. Thus this type of the SLE analysis has been routinely utilized for the analysis of the MFE and chemically induced dynamic electron and nuclear polarizations (CIDEP and CIDNP).[25–30] However one cannot calculate the time evolutions of the density matrix with the final value theorem. It is obvious that the SLE analysis on the time evolution (t-curve) of the MFE is helpful to obtain the detailed information on the RP dynamics including the diffusion process.

The SLE studies on the t-curve have been reported to clarify the mechanism of the MFE observed in the uniform solvents where the RP lifetime is on the order of nanosecond.[4,31,32] The effects of the hyperfine coupling constant and of the Δg on the recombination reactions in RP in the absence and presence of the magnetic fields (MFE due to the hyperfine coupling and Δg mechanism) are qualitatively studied by using the SLE. It has been shown that the coherent spin motions induced by the hyperfine coupling and the Δg effects convert the singlet RP to the triple RP, and vice versa and the MFEs are generated within a ten nanoseconds. However there are few SLE studies in which the experimental observations of the t-curve are fitted qualitatively to extract the diffusion parameters on RP. This is because the SLE analysis is time-consuming method when one employs the realistic molecular parameters. The large number of the hyperfine coupling constants and huge number of the grids for the RP diffusion description should be incorporated to describe the MFE phenomena with the realistic RP molecules. Both increase the number of columns and rows in the density matrix and prolong the computing time drastically. Since one needs to examine the various parameter sets to fit the experimental data, fitting of the experimental data remains a difficult task.

When RPs are generated in nano-structured materials, RPs have lifetimes longer than hundreds nanosecond due to the restriction of the RP diffusions. RPs in nano-structure materials therefore have enough time to change the spin states by the spin relaxations in the absence of the magnetic field. As the RP lifetime is prolong from nanoseconds to hundred nanoseconds, the mechanism of the MFEs is gradually switched from the combination of the hyperfine coupling and the Δg mechanisms to the spin relaxation mechanism.[33] In the time regions longer than hundreds nanoseconds, the spin coherence motions caused by the hyperfine coupling and the Δg effects are averaged by the translational and rotational diffusions of the solute molecules. The spin dynamics can be approximately represented by the incoherent spin conversion rate associated with the spin relaxations[33] and the coherent spin dynamics become less important. In this situation, it may be not necessary to incorporate all the hyperfine coupling constants into the calculation and one can use the SLE analysis for fitting of the t-curve due to the calculation times shortened.

We report herein a SLE analysis on the t-curve of the MFEs generated in the nano-structured materials where the RP lifetime is longer than hundred nanoseconds. The procedure of our SLE analysis follows the SLE reported by Pedersen and Freed[22–24] except the inverse Laplace transformation process. Instead of the final value theorem, Miller-Guy method[34] is employed for the inverse Laplace transformation to calculate the time evolution of the RP dynamics. To reduce the calculation time, only one hyper fine coupling constant is took into account while the diffusion motion of the RP is treated by the simple Brownian motion. The results show that the method proposed in the present study can correctly calculate RP dynamics and can be used for the simulation of the MFE data. When the coherent spin dynamics in RP is not important for the MFE generation, one can calculate the t-curve within a short time. Therefore it is possible to fit the t-curve of the MFE as well as the B-curve of the MFE by examining the various parameters sets. Our analysis demonstrates that fitting of both of the t-curve and the B-curve of the MFE data provide the detailed information on the diffusion parameters of RPs in nano-structured materials.

Methods

Stochastic Liouville equation and Laplace transformation

In the present study, we employed the Pedersen-Freed type SLE[22–24] to describe the RP dynamics. The SLE includes the spin-spin interactions, the molecular diffusions, the recombination reactions at the contact RP, and the spin relaxations as follows,

$$\frac{\partial \rho(r,t)}{\partial t} = -iH(r)^{\times}\rho(r,t) + D\Gamma_r \rho(r,t) + K_r \rho(r,t) + R_r \rho(r,t) \tag{1}$$

In this equation, $H(r)^{\times}$ is the commutator associated with the spin Hamiltonian $H(r)$ at the radical–radical distance r. $\rho(r, t)$ is the density matrix of RP at time t and distance r. D and Γ_r are the mutual diffusion coefficient and the diffusion operator, respectively. K_r and R_r are the superoperators for the recombination reactions and the spin relaxations, respectively.

The spin Hamiltonian is composed of the Zeeman interactions for the radicals, the hyperfine interactions between electron and nuclear spins with a hyperfine coupling constant (A), the r-dependent exchange interaction (J) and electron-electron dipole coupling Hamiltonian (H_{dd}),

$$H(r) = \mu_B \hbar^{-1} B(g_a S_{az} + g_b S_{bz}) + A\mathbf{S}_a\mathbf{I}_a - J(r)\left(\frac{1}{2} + 2\mathbf{S}_a\mathbf{S}_b\right) + H_{dd} \tag{2}$$

Here, $\mathbf{S}$ and $\mathbf{I}$ represent the electron and the nuclear spin operators, respectively. Subscripts a and b denote the individual radicals. g_a and g_b are the isotropic g-factor for radical a and b, respectively. In the present analysis, one magnetic nucleus in

radical a is included. The J gives the energy gap between the singlet and triplet states and is exponentially decayed with r as follows,

$$J = J_0 \exp[\gamma(r-d)] \tag{3}$$

where J_0 is a magnitude of the exchange interaction (J) at the closest distance d and γ is an exponential decay constant in r. The original SLE proposed by Pedersen and Freed was developed for the analysis on the CIDEP and CIDEP generated in solutions and does not include the dipole-dipole interaction because the dipole-dipole interaction averages to zero in solution where molecules are rotating freely.[22–24] Theoretical studies however suggested that the dipole-dipole interaction affects the spin dynamics by giving the energy gap between the spin state and by enhancing the spin relaxations even in solutions.[35–38] In the present study, the spin Hamiltonian in RP also includes dipolar coupling Hamiltonian of H_{dd}. H_{dd} is generally dependent on r and orientation of RP (Ω),

$$H_{dd}(r,\Omega) = \frac{\mu_0}{4\pi\hbar}\frac{g_a g_b \mu_B^{\ 2}}{r^3}\left[\mathbf{S}_a\mathbf{S}_b - \frac{3}{r^2}(\mathbf{S}_a\mathbf{r}_{ab})(\mathbf{S}_b\mathbf{r}_{ab})\right] \tag{4}$$

where $\mathbf{r}_{ab}$ is the vector connecting between two electron spins. In eqn (1), the angular dependence of the SLE is integrated out to simplify the calculations. The spin Hamiltonian in eqn (1) is therefore Hamiltonian averaged with respect to Ω and only dependent on r. For conveniently we use the following dipole coupling parameter in the r-dependent spin Hamiltonian,[38]

$$D^d(r) = -\frac{3}{2}\frac{\mu_0}{4\pi}\frac{g_a g_b \mu_B^{\ 2}\hbar}{r^3} \tag{5}$$

Eqn (5) gives the energy gap between the triplet spin states even in the absence of the magnetic field. Eqn (5) also accounts the fluctuations of dipole coupling parameters caused by the translational diffusion motion of RP. Such fluctuations of dipole coupling induce the spin relaxations in RP. In solutions, the dipole coupling is also fluctuated by the rotational motion of RP. This effect is taken into account as magnetic field dependent spin relaxations in RP. The details of the spin relaxation operators are described later.

The Laplace transform of eqn (1) is

$$s\hat{\rho}(r,s) - \rho(r,t=0) = -iH(r)^{\times}\hat{\rho}(r,s) + D\frac{\partial^2}{\partial r^2}\hat{\rho}(r,s) + K\hat{\rho}(r,s) + R\hat{\rho}(r,s) \tag{6}$$

where

$$\hat{\rho}(r,s) \equiv \int_0^\infty \exp(-st)r\rho(r,t)dt \equiv \int_0^\infty \exp(-st)r\hat{\rho}(r,t)dt \tag{7}$$

The time dependent RP population ($\mathcal{P}_{RP}(t)$) is defined as,

$$\mathcal{P}_{RP}(t) = \mathrm{Tr}\rho(t) \tag{8a}$$

$$\rho(t) \equiv \int_d^\infty r\hat{\rho}(r,t)dr \tag{8b}$$

The diffusion of the radical in RP is treated as simple Brownian motion with finite difference technique as follows,

$$D\frac{\partial^2\hat{\rho}(r,s)}{\partial r^2} = D\frac{\hat{\rho}(r-\Delta r,s) - 2\hat{\rho}(r,s) + \hat{\rho}(r+\Delta r,s)}{\Delta r^2} \tag{9}$$

where Δr is small but finite increment in r. The application of the finite difference technique is essentially equivalent to transforming the continuous diffusion equation into the discrete master equation involving the transition probability matrix $\mathbf{W}$. The $\mathbf{W}$ couples $\rho(r,t)$ between discrete values $\rho(r_0+j\Delta r,\ t)$ where j = 0,1,2,...., L when the one Δr value is used. These discrete value form a column vector $\boldsymbol{\rho}$.

$$D\frac{\partial^2\hat{\rho}}{\partial r^2} \rightarrow \mathbf{W}\hat{\boldsymbol{\rho}} \tag{10}$$

In the analysis, we set needed segments in the distance r from the closest distance of d. The Δr values were Δr_1= 0.01 nm in the first 16 segments, Δr_2= 0.02 nm in the second 16 segments, and Δr_3= 0.05 nm in the third segments. The number of the third segments was a variable parameter in fitting process. Thus the total number (L) of the segments was also variable in the analysis. With the finite difference technique, we approximate the integral in eqn (8b),

$$\int_d^\infty r\hat{\rho}(r,t)dr = \sum_{j=0}^{L} V(j)\hat{\rho}(j,t) \tag{11}$$

where $V(j)$ is the radial weighting factor for the jth position.

The mutual diffusion coefficient D is a sum of the diffusion coefficients of radical a and b: D=D_a+D_b. In our analysis, D_a and D_b are determined by using Stokes-Einstein equation as follows,

$$D_a = \frac{k_B T}{6\pi\eta d_a},\ D_b = \frac{k_B T}{6\pi\eta d_b} \tag{12}$$

where η is the viscosity for the RP diffusion area and d_a and d_b is the radii of the radical a and b, respectively.

In the present study, we employed a cage model[27,28] to reproduce the MFE observed in the micellar solution. In the cage model, the RP diffusion is restricted by the spherical cage with the radius of R. The one radical is fixed to the center of the sphere and the other radical is freely diffused with the viscosity η in the spherical cage. At the contacted RP, RP is recombined with a rate constant of k_{rec}. When the radical reaches the interface of the cage, the radical escapes from the cage with a probability of P_{esc}. Once the radical escapes, it cannot diffuse back to the inside of the cage. In the SLE analysis, the terms of $\mathbf{W}_{L,L}$ and $\mathbf{W}_{L+1,L}$ determine the escape rate of RP from the cage and represented as,

$$\mathbf{W}_{L,L} = \frac{-\{k_{out}(1+\Delta r_3/r) + k_{in}(1-\Delta r_3/r)\}}{\Delta r_3^{\ 2}} \tag{13a}$$

$$\mathbf{W}_{L+1,L} = \frac{k_{\text{out}}}{\Delta r_3^{\,2}} \tag{13b}$$

where k_{in} is equivalent with D and the escape rate of the RP (P_{esc}) at the interface is defined as $P_{\text{esc}}=k_{\text{in}}/k_{\text{out}}$. In the simulation, RP is collected at the last segments and cannot diffuse back.

The recombination reaction operator is described as,

$$K_r\hat{\rho}(r,s) = -\frac{k_{\text{rec}}(r)}{2}\left[|\mathrm{S}\rangle\langle\mathrm{S}|\hat{\rho}(r,s) + \hat{\rho}(r,s)|\mathrm{S}\rangle\langle\mathrm{S}|\right] \tag{14}$$

We assumed that RP is recombined with the rata constant of k_{rec} at the closest distance with the reaction zone of 0.05 nm. In other r regions, the recombination reactions were assumed not to proceed and the values of $k_{\text{rec}}(r)$ were set to be 0.

The form of the spin relaxation matrix used in SLE is described in the literature[39]and also in Supplemental Information. The longitudinal relaxation rate constant $(1/T_1)_{\text{radical}}$ for the radicals is represented as,[2,40]

$$\left(\frac{1}{T_1}\right)_{\text{radical}} = \frac{3(\delta g_{\text{a}}\times\mu_{\text{B}}B)^2 + (\delta A\times g_{\text{a}}\mu_{\text{B}})^2}{30\hbar^2}\times\frac{\tau_{\text{a}}}{1+\omega^2\tau_{\text{a}}^{\,2}} + \frac{3(\delta g_{\text{b}}\times\mu_{\text{B}}B)^2}{30\hbar^2}\times\frac{\tau_{\text{b}}}{1+\omega^2\tau_{\text{b}}^{\,2}} \tag{15}$$

where δg_{a} and δg_{b} are anisotropies for the g-factors for radical a and b, respectively. δA is the anisotropy for the hyperfine coupling constant. ω is the energy splitting for the spin states associated with the spin relaxations. τ_{a} and τ_{b} are the rotational correlation time for radical a and b, respectively, and represented as follows,

$$\tau_{\text{a}} = \frac{4\pi\eta d_{\text{a}}^{\,3}}{3k_{\text{B}}T},\quad \tau_{\text{b}} = \frac{4\pi\eta d_{\text{b}}^{\,3}}{3k_{\text{B}}T} \tag{16}$$

For the T-T relaxation, $\omega=g\mu_{\text{B}}h^{-1}B+|D^{\text{d}}(r)/2\pi|$ is used while $\omega=g\mu_{\text{B}}h^{-1}B+|2J(r)/2\pi|$ is used for the S-T_- and S-T_+ relaxations. In the presence of the large J value in the closed RP, the transverse relaxation rate constant $(1/T_2)$ for the S-T_0 relaxation may be represented as,

For $2J(r)>\delta g_{\text{a}}\times\mu_{\text{B}}B/\hbar$, $2J(r)>\delta g_{\text{b}}\times\mu_{\text{B}}B/\hbar$, and $2J(r)>\delta A\times g_{\text{a}}\mu_{\text{B}}/\hbar$,

$$\frac{1}{T_2} = \frac{3(\delta g_{\text{a}}\times\mu_{\text{B}}B)^2 + (\delta A\times g_{\text{a}}\mu_{\text{B}})^2}{30\hbar^2}\times\frac{\tau_{\text{a}}}{1+\left[2J(r)/2\pi\right]^2\tau_{\text{a}}^{\,2}} + \frac{3(\delta g_{\text{b}}\times\mu_{\text{B}}B)^2}{30\hbar^2}\times\frac{\tau_{\text{b}}}{1+\left[2J(r)/2\pi\right]^2\tau_{\text{b}}^{\,2}} \tag{17}$$

When the S and T_0 state is nearly degenerated, on the other hand, $1/T_2$ may be represented as,

For $2J(r)<\delta g_{\text{a}}\times\mu_{\text{B}}B/\hbar$, $2J(r)<\delta g_{\text{b}}\times\mu_{\text{B}}B/\hbar$, and $2J(r)<\delta A\times g_{\text{a}}\mu_{\text{B}}/\hbar$,

$$\frac{1}{T_2} = \frac{3(\delta g_{\text{a}}\times\mu_{\text{B}}B)^2 + (\delta A\times g_{\text{a}}\mu_{\text{B}})^2}{30\hbar^2}\times 4\tau_{\text{a}} + \frac{3(\delta g_{\text{b}}\times\mu_{\text{B}}B)^2}{30\hbar^2}\times 4\tau_{\text{b}} \tag{18}$$

For the T-T relaxation, the following longitudinal relaxation rate constant due to the dipole interactions is added,[2]

$$\left(\frac{1}{T_1}\right)_{\text{RP}} = \frac{\mu_{\text{B}}^{\,4}g_{\text{a}}^{\,2}g_{\text{b}}^{\,2}}{10\hbar^2r^6}\times\frac{3\tau_{\text{ab}}}{1+\omega^2\tau_{\text{ab}}^{\,2}} \tag{19a}$$

$$\tau_{\text{ab}} = \frac{4\pi\eta r^3}{3k_{\text{B}}T} \tag{19b}$$

The complete solution given by eqn (6) becomes the matrix equation,

$$[s1-\mathbf{K}'-\mathbf{W}'-\mathbf{R}'+i\boldsymbol{\Omega}]\hat{\boldsymbol{\rho}}(s) = \hat{\boldsymbol{\rho}}(0) \tag{20}$$

One solves matrix eqn (20) for the elements of $\hat{\boldsymbol{\rho}}(s)$. The detail of the SLE analysis is described in Supplemental Information.

Inverse Laplace Transformation by Miller-Guy Method.[34]

$\hat{\boldsymbol{\rho}}(s)$ corresponds to the set of the density matrix elements in the frequency domain. For the MFE calculation, one needs the density matrix elements in the time domain $\hat{\boldsymbol{\rho}}(t)$. Thus, $\hat{\boldsymbol{\rho}}(s)$ has to be recovered to $\hat{\boldsymbol{\rho}}(t)$ by the inverse Laplace transformation.

For the inversion of the Laplace transform, we change the variable from t to x. The variable integration may be changed by the substitution.

$$x = 2\exp(-\delta t) - 1 \tag{21}$$

For δ, one should select the appropriate number to give the correct answer. Basically the δ value close to $1/t$ seems to be appropriate. If this equation is solved for t, then

$$t = -\left(\frac{1}{\delta}\right)\log\left(\frac{x+1}{2}\right) \tag{22}$$

t in eqn (22) is substituted to $\hat{\rho}(r,t)$,

$$\hat{\rho}(r,t) = \hat{\rho}\left\{r,\left[-\left(\frac{1}{\delta}\right)\log\left(\frac{x+1}{2}\right)\right]\right\} = g(r,x) \tag{23}$$

$\hat{\rho}(r,t)$ is now the function of x and is represented as $g(r,x)$. t in eqn (22) is also substituted to $\exp(-st)$,

$$\exp(-st) = \left(\frac{x+1}{2}\right)^{\frac{s}{\delta}} \tag{24}$$

Differentiation of time t by x (eqn (22)) gives the following equation,

$$\frac{dt}{dx} = -\frac{1}{\delta}\times\frac{1}{2}\times\frac{2}{x+1} = -\frac{1}{\delta}\times\frac{1}{2}\times\left(\frac{x+1}{2}\right)^{-1} \tag{25}$$

Substitution of eqn (23)-(25) into eqn (7) gives,

$$\hat{\rho}(r,s)=\left(\frac{1}{2\delta}\right)\int_{-1}^{1}\left(\frac{x+1}{2}\right)^{\left(\frac{s}{\delta}-1\right)}g(r,x)dx \tag{26}$$

According to eqn (22), the values of t=0 and t=∞ give the values of x=1 and x=-1, respectively. The function $g(r,x)$ in eqn (26) is expanded over -1≤x≤1 in terms of the Jacobi polynomials,[41]

$$g(r,x)=\sum_{n=0}^{\infty}C_n(r)P_n^{(0,\beta)}(x) \tag{27a}$$

$$P_n^{(0,\beta)}(x)=\frac{(-1)^n}{2^n n!}(1-x)^{-\beta}\frac{d^n}{dx^n}\left[(1-x)^n(1+x)^{n+\beta}\right] \tag{27b}$$

where $C_n(r)$ are undetermined coefficients, β is an integer which should be chosen to give the correct answers, and $P_n^{(\alpha,\beta)}(x)$ is a Jacobi polynomials. In the present study, β=0 was used in the all calculations. If the coefficients $C_n(r)$ are known, then g(r,x) is known, which implies that $\hat{\rho}(r,t)$ can be calculated by means of eqn (23). The next step is to obtain the coefficient $C_n(r)$ to calculate $g(r,x)$ according to eqn (27). Substitution of eqn (27) into eqn (26) results in,

$$\hat{\rho}(r,s)=\left(\frac{1}{2\delta}\right)\int_{-1}^{1}\left(\frac{x+1}{2}\right)^{\left(\frac{s}{\delta}-1\right)}\left[\sum_{n=0}^{\infty}C_n(r)P_n^{(0,\beta)}(x)\right]dx \tag{28}$$

By substituting s=(β +1+k)δ into the previous equation and simplifying terms one has,

$$\delta\hat{\rho}[r,(\beta+1+k)\delta]=\left(\frac{1}{2}\right)^{(\beta+k+1)}\int_{-1}^{1}(1+x)^{(\beta+k)}\left[\sum_{n=0}^{\infty}C_n(r)P_n^{(0,\beta)}(x)\right]dx \tag{29}$$

k is a positive integer. By the expansion the term of (1+x)k into the series and the use of integral transforms,[42] we can finally get the following relation,

$$\delta\hat{\rho}[r,(\beta+1+k)\delta]=\sum_{n=0}^{k}C_n(r)\frac{\Gamma(k+\beta+1)k!}{(k-n)!\Gamma(k+\beta+n+2)} \tag{30a}$$

$$\Gamma(z)=(z-1)! \tag{30b}$$

Here k also determines the number of coefficient $C_n(r)$. In the present study, we used value of k=12 in all calculations. By changing k value as 0, 1, 2, 3, 4⋯ , one obtain (k+1) sets of equations from eqn (30). The left side of eqn (30a) is obtained by the density matrix in s-domain using eqn (20) with the relation of s=(β+1+k)δ. The obtained liner equation can be solved with the general procedure. Thus the coefficient $C_n(r)$ can be determined. Since x=2exp(-δt)-1, the Jacobi polynomials may be expressed as functions of t directly. From eqn (21), (23) and (27), the function of $\hat{\rho}(r,t)$, which is the inverse Laplace transformation of $\hat{\rho}(r,s)$, is represented as,

$$\hat{\rho}(r,t)\approx\sum_{n=0}^{k}C_n(r)P_n^{(0,\beta)}[2\exp(-\delta t)-1] \tag{31}$$

When the terms of n and n+β are nonnegative integers, the Jacobi polynomial can be written as,[41]

$$P_n^{(0,\beta)}(x)=n!(n+\beta)!\times\sum_q\left[q!(n-q)!(\beta+q)!(n-q)!\right]^{-1}\left(\frac{x-1}{2}\right)^{n-q}\left(\frac{x+1}{2}\right)^{q} \tag{32}$$

where q is positive integer and summation extends to q values which satisfy the relation of n-q≥ 0. The time dependent RP population, $\mathcal{P}_{RP}(t)$, is given by,

$$\mathcal{P}_{RP}(t)=\sum_{j=0}^{M}V(j)\left[\hat{\rho}_{S,S}(j,t)+\hat{\rho}_{T+,T+}(j,t)+\hat{\rho}_{T_0,T_0}(j,t)+\hat{\rho}_{T_-,T_-}(j,t)\right] \tag{33}$$

RP is generated by the photochemical reactions with the rate constant of k_{gen}. To reproduce the experimental results, the obtained $\mathcal{P}_{RP}(t)$ was convoluted with k_{gen}.

$$\mathcal{P}_{RP}(t)'=\int_0^{\infty}\exp(-k_{gen}\tau)\mathcal{P}_{RP}(t-\tau)d\tau \tag{34}$$

We examined two methods, method **1** and **2** (Fig. 1) to evaluate the above procedure for the t-curve calculations. In method **1**, the time dependences of the density matrix are directly calculated from the initial condition of the density matrix by changing the t value. One only calculates the density matrix elements needed for the analysis therefore one can save the calculation time. In method **2**, the density matrix is calculated with a fixed small time increment Δt. First the density matrix at time t is calculated from the initial condition of the density matrix. Then the density matrix at time 2t is calculated from the density matrix at time t. By repeating this procedure, one obtains the time dependence of the density matrix. In method **2**, one should calculate the all elements in the density matrix since the set of the density matrix is necessary for the next time step calculations. Though the calculation accuracy in method **2** may be greater than that in method **1**, one needs the longer calculation time in method **2**.

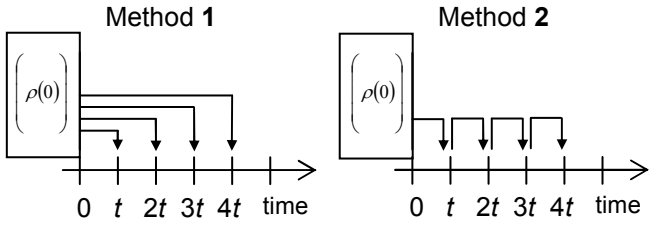

Fig. 1 Schematic representations for calculation methods used in the present study. In method **1**, the time dependences of the density matrix are directly calculated from the initial condition of the density matrix $\rho(0)$. In method **2**, the time dependences of the density matrix are calculated by a recurrence equation manner with a fixed time increment t. For example the density matrix at time 2t was calculated from the density matrix at time t

Results and Discussions

Test of SLE program

The simple calculations were performed to test the abilities of the inverse Laplace transformation procedures for the calculations of the time evolutions of the MFEs. We examined how the time dependence of the RP populations are influenced by the effects of the recombination reaction, the spin relaxations, the diffusion and the spin interactions included in the spin Hamiltonian. For this purpose, the SLE of eqn (1) was modified to the specialized SLE where only one term in the right hand side of eqn (1) is included and other three terms are omitted. Fig. 2 shows time dependences of the RP populations calculated by using the SLE specialized in the recombination reaction (Fig. 2a), in the transverse spin relaxation (Fig. 2b), and in the longitudinal spin relaxation (Fig. 2c). The singlet RP state is initially populated and the recombination reaction or the spin relaxations occur from the singlet RP state. A rate constant of 1×10^7 s^{-1} is used for the recombination reaction rate and the spin relaxation rates. The calculations are performed with method **1** and method **2.** Both methods give the identical results. As can be seen in Fig. 2a, the singlet RP decays with the rate constant of 1×10^7 s^{-1} by the recombination reaction. In the SLE calculations with the spin relaxations (Fig. 2b and 2c), the singlet RPs also decay with the rate constant of 1×10^7 s^{-1} whereas the triple RPs are increased with the rate constant of 1×10^7 s^{-1}. The population of the singlet RP decreases to 0.5 for the calculation with the transverse spin relaxation and to 0.25 for the calculation with the longitudinal spin relaxation as is expected from the number of the spin states associated with the spin relaxations. Simultaneously, the population of the triplet RP increases to 0.5 and 0.75 in the presence of the transverse and longitudinal spin relaxations, respectively. The transverse spin relaxation involves the S and T_0 states while the longitudinal spin relaxation involves the S, T_+, T_0 and T_- states. The results indicate that method **1** and **2** can calculate the time evolutions of the RP populations caused by the spin relaxations and the recombination reaction perfectly.

We also examined how the recombination process from the triplet state is modulated by the transverse and longitudinal spin relaxations in RP. In the calculations, the SLE only includes the spin relaxation and recombination terms. In the initial states, the three triplet states in RP were equally populated. The recombination reaction occurred from the singlet state. The transverse or longitudinal spin relaxation rate was set to be 1×10^7 s^{-1} while the recombination reaction rate was 1×10^{10} s^{-1}. In this parameter set, obviously, the rate determining step of the recombination process is the spin relaxation in RP. Fig. 3 show time dependences of RP population ($\Phi_{RP}(t)$) calculated in the presence of the spin relaxation and the recombination reaction. In Fig. 3, time dependences of the singlet and triplet RP populations caused by the spin relaxations in the absence of the recombination reactions are also shown. When the transverse spin relaxation occurs with the rate constant of 1×10^7 s^{-1}, $\Phi_{RP}(t)$ decays with a rate constant of 0.5×10^7 s^{-1}. When the longitudinal spin relaxation rate is 1×10^7 s^{-1}, $\Phi_{RP}(t)$ decays with a rate constant of 0.25×10^7 s^{-1}. Though the rate determining step is the spin relaxation processes, the spin relaxation rate does not directly give the rate of the recombination process. In RP, the spins are relaxed to achieve the thermal equilibrium where the populations of the spin sates associated with the spin relaxation are approximately the same. On the other hand, RP recombines only from the singlet state. Therefore one needs to consider the number of the spin states involved in the spin relaxations of RP. When the rate determining step is the spin relaxations rate ($1/T$), the rate of the recombination process is given by $(1/T)\times(M_{rec}/M_{all})$ where M_{rec}, and M_{all} are the number of the spin states in which the recombination occurs, and the number of all spin states associate with the spin relaxations, respectively. In the transverse spin relaxation, the number of the spin states associated with the relaxation is two (S and T_0) while that is four (S, T_+, T_0, T_-) for the longitudinal spin relaxation process. Thus the rates of the recombination from the triplet RP induced

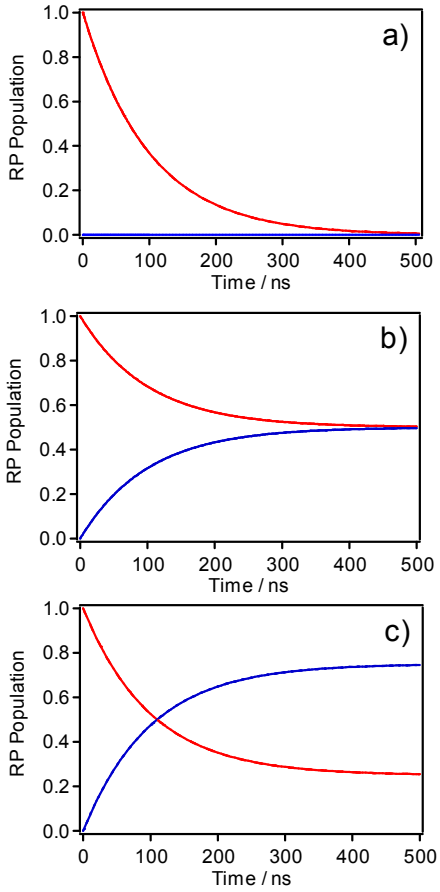

Fig. 2 Time evolutions of populations of singlet (red lines) and triplet (blue lines) radical pairs calculated by method **1** (solid lines) and method **2** (dashed lines) with an initial condition of a pure singlet radical pair. The calculations are specialized (a) in a recombination reaction from singlet, (b) a transverse spin relaxation and (c) a longitudinal spin relaxation with a rate constant of 1×10^7 s^{-1}. In all calculations, method **1** and **2** give identical results.

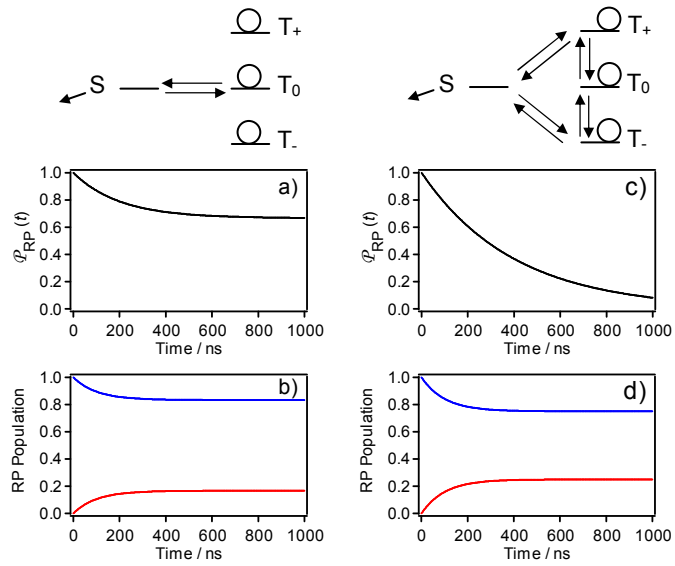

Fig. 3 Time evolutions of radical pair population ($\mathcal{P}_{RP}(t)$) calculated in the presence of spin relaxations and recombination reaction from the singlet state. An initial condition is triplet sate where the three triplet states are equally populated. (a) $\mathcal{P}_{RP}(t)$ calculated with a transverse spin relaxation rate constant of 1×10^{7} s^{-1} and recombination reaction rate of 1×10^{10} s^{-1}. (b) Time evolutions of populations of singlet (red lines) and triplet (blue lines) radical pair calculated with a transverse spin relaxation rate constant of 1×10^{7} s^{-1} in the absence of the recombination reaction. (c) $\mathcal{P}_{RP}(t)$ calculated with a longitudinal spin relaxation rate constant of 1×10^{7} s^{-1} and recombination reaction rate of 1×10^{10} s^{-1}. (d) Time evolutions of populations of singlet (red lines) and triplet (blue lines) radical pair calculated with a longitudinal spin relaxation rate constant of 1×10^{7} s^{-1} in the absence of the recombination reaction.

by the transverse spin relaxation and the longitudinal spin relaxation are represented as $(1/T)\times1/2$ and $(1/T)\times1/4$, respectively.

Next the diffusion motion of RP in the SLE calculations was examined. Here we employed the uniform solvent model rather than the cage model for simplicity. The two radicals with the radius of 0.3 nm initially form the contacted RP at the separation of r = 0.6 nm. After the generation of the contacted RP, the RP diffuses freely by the simple Brownian motion. The viscosity was set to be 1 cP, assuming the common organic solvents. These parameters give the value of D=1.4×10^{-9} m^{2}s^{-1} for the mutual diffusion coefficient. Fig. 4a shows r distribution of RPs calculated by method **1** at the delay time of 0.1 ns and 1 ns after the generation of the contacted RP. The maximum RP population is obtained at r = 1.2 nm with the delay time of 0.1 ns. At the delay time of 1 ns, the r value for the maximum RP population is shifted to 2.5 nm and the distribution of r becomes broader as expected. The calculated results are evaluated by using the mean square distance ($\langle r_{MS}^2 \rangle$) of diffusing particle in time t. By the simple diffusion model, the $\langle r_{MS}^2 \rangle$ value is represented with the delay time of t and the diffusion coefficient of D as follows,[43,44]

$$\left\langle r_{MS}^{\ 2} \right\rangle = 2NDt \qquad (35)$$

where N represents the dimension for the diffusion and we used value of N=3 in the present calculations. In our program, r does not directly give the diffusion distance of the radicals. The diffusion distance of the radicals can be estimated from the value of r-d therefore $\langle (r-d)^2 \rangle$ corresponds to $\langle r_{MS}^2 \rangle$ in the present analysis. At the various delay time t, we obtain the values of $\langle (r-d)^2 \rangle$ from the r distributions of the RPs calculated. Fig. 4b shows t dependence of $\langle (r-d)^2 \rangle$ obtained by our computer calculation. The good liner relationship between $\langle (r-d)^2 \rangle$ and t suggests that eqn (35) well holds in the analysis. The D value is estimated to be 1.4×10^{-9} m^{2}s^{-1} from the slop of t dependence of $\langle (r-d)^2 \rangle$ by using eqn (35). The estimated value is equal to the D value inputted to the computer calculations, indicating the validity of the diffusion motions of RPs calculated by method **1**. Fig. 4c shows time dependences of $\mathcal{P}_{RP}(t)$ at r = 1.2 nm calculated by method **1** and method **2**, respectively. Around time 0, RP at r = 1.2 nm is not populated because RP is initially contacted and can not reach the

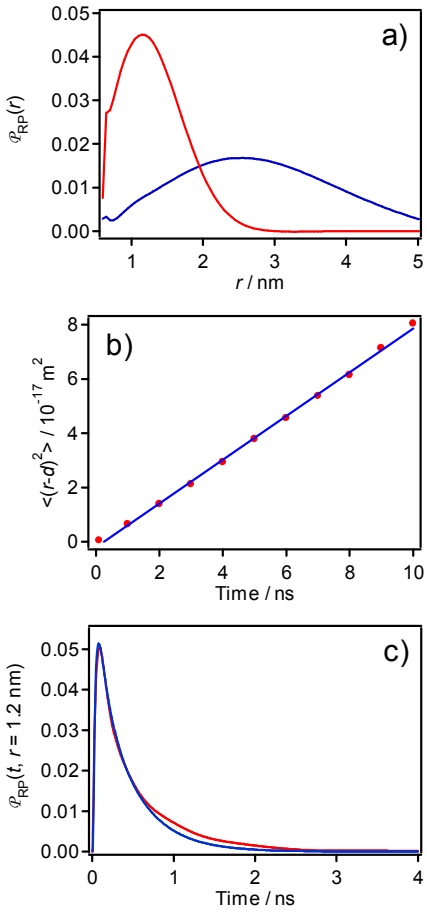

Fig. 4 Time evolutions of radical pair populations ($\mathcal{P}_{RP}(t)$) obtained by calculations specialized diffusion motion of radical pairs with an initial condition of contacted radical pairs (r = 0.6 nm) and the parameter of D=1.4×10^{-9} m^{2}s^{-1}. (a) r distribution of radical pairs calculated by method **1** at the delay time of 0.1 ns (red line) and 1 ns (blue line). (b) Delay time dependence of mean square distance ($\langle r_{MS}^2 \rangle$, red circle) obtained by radical pair distributions calculated by method **1**. Blue line shows least square fit. (c) Time evolution of the RP population at r = 1.2 nm calculated by method **1** (red line) and method **2** (blue line).

distance of r = 1.2 nm. With the increase of time, the population of RP at r = 1.2 nm is increased by the diffusion motion and $\mathcal{P}_{RP}(t)$ have the maximum at the delay time of 0.1 ns. The RP populations gradually decrease after the delay time of 0.1 ns. The results obtained by method **1** are slightly different from the results obtained by method **2** in the time region of 0.5 ns < t < 2.5 ns. The results suggest that one must be careful to choose the δ value in eqn (21) for the calculation of method **1**. Nevertheless, both method **1** and method **2** give the similar results for the diffusion motion of RPs.

As can be seen in Fig. 2 and 4, the RP dynamics calculated by method **1** and method **2** are in good agreement with that obtained by the simple expectations and the analytical formula and we concluded that the inverse Laplace formation by method **1** and method **2** sufficiently functions to describe the time variation of the RP distributions caused by the recombination reactions, the spin relaxations and the diffusion motion in which the time dependence of the RP populations can be approximately represented by the exponential function with the real exponents.

Finally, the time dependences of the RP populations were calculated with the spin Hamiltonian including the hyperfine interaction or the Δg effect. The precursor of the spin states was set to be a pure singlet state. In order to check the results obtained by method **1** and method **2**, the time dependences of the RP populations were also evaluated by integrating the Liouville-von Neumann equation with the time independent spin Hamiltonian,[45]

$$\rho(t) = \exp(-iHt)\rho(0)\exp(iHt) \qquad (36)$$

In the calculations, we used the value of J=0 and D^{d}=0 to make the calculated results easy to understand. Fig. 5 shows time dependences of the singlet RP populations calculated with the hyperfine interaction of 0.5 mT in the absence (Fig. 5a) and presence (Fig. 5b) of the magnetic field of 1 T and with the Δg effects (Δg = 0.001) in the presence of the magnetic field of 1 T (Fig. 5c). In the presence of the external and intramolecular local magnetic field, the spins precess with respect to the quantization axis and the system starts to oscillate. The singlet state is mixed to the triplet states and the population of the singlet RP shows oscillatory behaviour with respect to the time. In the absence of the magnetic field, three of four spin states are mixed by the hyperfine interaction, giving the eigenstates energetically separated by the magnitude of the hyperfine coupling constant. As can be shown in Fig. 5a, the singlet RP population oscillates with the frequency equal to the hyperfine coupling constant (0.5 mT ≈ 1.4 × 10^7 s^{-1} ≈70 ns) as expected. Since the spin Hamiltonian is constructed with the high field approximation in the present study, the calculated RP dynamics may be somewhat different from the real spin dynamics in the absence of the magnetic field. In the presence of the magnetic field of 1 T, the frequencies for the oscillations correspond to the difference in the EPR resonant lines between two radicals and are determined by the half of the hyperfine coupling constant (0.25 mT ≈ 7 × 10^6 s^{-1} ≈35 ns) or the Δg effects (1.4 ×10^7 s^{-1} ≈ 70 ns). The SLE calculations by method **2** give the

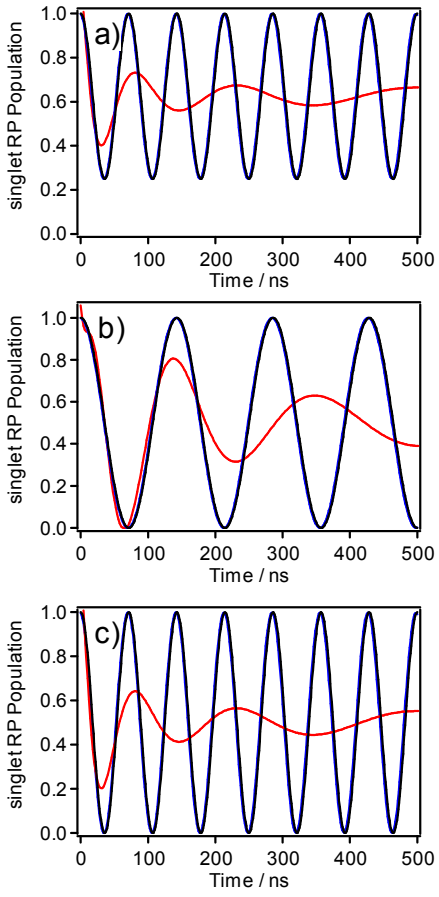

Fig. 5 Time evolutions of singlet radical pair populations calculated with spin Hamiltonian by method **1** (red lines) and method **2** (blue lines). The calculations were performed with an initial condition of pure singlet radical pair and parameters of J=0 and D^{d}=0. The spin Hamiltonian consists of a hyperfine coupling constant of 0.5 mT in the absence (a) of and presence (b) of the magnetic field of 1 T. In (c), the spin Hamiltonian includes the Δg effect (Δg = 0.001) in the presence of the magnetic field of 1 T whereas the hyperfine coupling constant is not included. Time evolutions of populations of singlet radical pairs calculated by eqn (36), which are identical with the calculation by method **2** (blue lines), are also depicted by black lines.

identical results with the calculations by eqn (36), indicating that method **2** can correctly calculate oscillatory spin dynamics. In the SLE calculations by method **1**, on the other hand, the oscillations are dumped with time and the populations finally settle on the averaged populations with respect to the time. These charactesristics are quite similar to the decoherence phenomena caused by spin relaxations[46] though the SLE does not include the sources of the spin relaxations in the present calculations. In addition to that, the frequencies for the oscillations are not constant in method **1** and slightly decrease with respect to the time. The results suggest that method **1** cannot be applied to the spin systems where the coherent oscillations play important roles. However it may be possible to apply method **1** to calculate the time dependence of the RP populations in the systems where the spin coherences are not important since method **1** only cause the decoherences and does not bring the serious artefacts.

Application to the MFEs Observed in the Micellar Solution

Micelles are well-known self-organized materials and provide the nanometer sphere like spaces for chemical reactions.[47,48] When RPs are generated in the micelles, RPs are often confined inside of the micelle. The RP lifetimes are prolonged to microseconds and the large MFEs have been observed in the micellar solutions.[10,49,50,10] Previously we reported the MFEs on the RP generated by hydrogen abstract reaction between photo-excited triplet of xanthone (XO) and xanthene (XH_2) in aqueous micellar solutions consisting of the surfactant of sodium dodecyl sulfate (SDS).[12] Under the various magnetic fields, the yield of the XO ketyl radical ($XOH^{\bullet}$) were evaluated by using a nano-second laser flash photolysis. Fig. 6 shows time profiles ($A(t)$) of the transient absorption observed at the wavelength of 490 nm in the absence and presence of the magnetic field of 4 T. The observed transient absorptions compose of the absorption due to the photo-excited triplet state ($^3XO^*$) of xanthone and the absorption of $XOH^{\bullet}$. The fast decay component within a few hundred nanoseconds can be ascribed to the decay of $^3XO^*$ and the transient absorptions after the delay time of 1 μs are associated with the absorption of $XOH^{\bullet}$. Apparently the yield of $XOH^{\bullet}$ is affected by the magnetic field. The $R(B)$ values on the yield of $XOH^{\bullet}$ were obtained by using the transient absorbance at the delay time of 15 μs after the laser excitation: $R(B) = Y(B\ \mathrm{T})/Y(0\ \mathrm{T}) = A(15\ \mu\mathrm{s}, B\ \mathrm{T})/A(15\ \mu\mathrm{s}, 0\ \mathrm{T})$. Fig. 7 shows a magnetic field dependence of $R(B)$ observed in the SDS micellar solutions, indicating the experimentally obtained B-curve. The $R(B)$ value increases with increasing B in the region of $0 < B < 1.5$ T and is saturated in 1.5 T $< B <$ 4 T. The observed MFEs are quite large, suggesting that the MFEs are caused by the spin relaxation mechanism and the RPs were confined in the micelles. To obtain the experimental t-curve, the time profile of the transient absorption observed at 0 T is subtracted from that observed at 4 T (Fig. 8). By the subtraction procedure, the contribution of $^3XO^*$ to the t-curve is cancelled out. The MFEs are generated within 1 μs and reaches the constant value at 2 μs.

To extract the parameters for the RP diffusion in the SDS micellar solution, we attempted simultaneous fitting of the t-curve and the B-curve of the MFE by using the SLE with the cage model. In the cage model, the RP diffusion is restricted by the spherical cage with the radius of R and inside viscosity η. When the radical reaches the interface of the cage, the radical escapes from the cage with the probability of P_{esc}. The detail of the cage model is described in the method section. For the initial condition, we assumed that RPs are populated with three triplet state (T_+, T_0, T_-) equally at the closest distance d. The core radius and hydrodynamic radius for the SDS micelle has been estimated to be 1.6 nm and 2.1 nm, respectively, from the molecular structure of SDS.[51,52] The η value in the SDS micelle were reported to be 9-36 cP.[53–57] Keeping these values in mind, fitting were performed by using method **1**. The best fit for both of t-curve and B-curve was obtained with parameter set **1**, which is listed in Table 1. The values of the other parameters such as k_{gen}, J_0, and γ used in fitting are described in Supplemental Information. We also examined other parameter set **2** and **3** to evaluate the fitting procedure proposed in the present study. In parameter set **2**, the η value is the same with that in parameter set **1** while R is extended from 1.7 nm to 2.5 nm. In parameter set **3**, on the other hand, we employ the value of η=10 cP and R is fixed to 1.7 nm. As is shown in Fig. 7, the

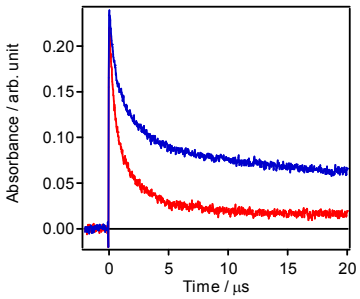

Fig. 6 Time profiles of transient absorption observed by a nanosecond laser flash photolysis at a wavelength of 490 nm in sodium dodecyl sulfate (SDS) micellar solution containing xanthone (0.5×10^{-3} mol dm^{-3}) and xanthene (1.0×10^{-3} mol dm^{-3}) in the absence of (red line) and presence (blue line) of a magnetic field of 4 T.[12]

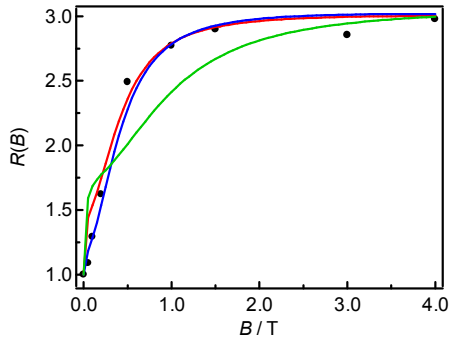

Fig. 7 Magnetic field effects on the yield of xanthone ketyl radical observed at 490 nm with a delay time of 15 μs in sodium dodecyl sulfate (SDS) micellar solution (black circles). Solid lines show fitting by method **1** with parameter set **1** (red line), parameter set **2** (blue line) and parameter set **3** (green line).

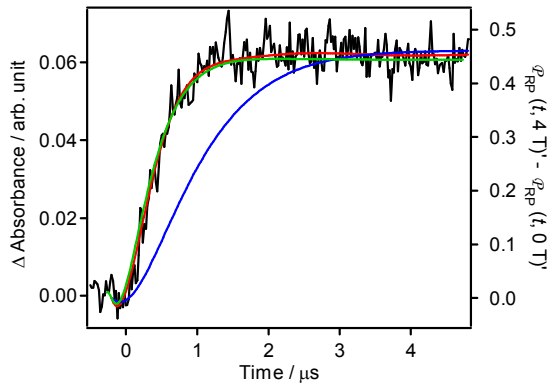

Fig. 8 Time evolution of magnetic field effect on the yield of the xanthone ketyl radical obtained by subtracting time profile of transient absorption in the absence of the magnetic field from that obtained in the presence of the magnetic field of 4 T (black line). Colored lines show fitting by method **1** with parameter set **1** (red line), parameter set **2** (blue line) and parameter set **3** (green line).

Table 1. Cage parameters used for the SLE analysis; viscosity (η) in the cage, mutual diffusion coefficient (D) for the radical pair in the cage, escape probability (P_{esc}) at the interface, radius (R) of the cage, recombination reaction rate (k_{rec}) at the closest radical-radical distance, respectively.

No	Cage Parameters				
	η / cP	D / m^2s^{-1}	P_{esc}	R / nm	k_{rec} / s^{-1}
1	30	4.8×10^{-11}	7.8×10^{-4}	1.7	1.0×10^{10}
2	30	4.8×10^{-11}	3.5×10^{-4}	2.5	3.5×10^{9}
3	10	1.1×10^{-8}	2.1×10^{-4}	1.7	1.0×10^{10}

calculations with parameter sets **1** and **2** can reproduce the *B*-curve observed in the SDS micellar solutions, whereas two parameter sets give the different *t*-curves as shown in Fig. 8. The parameter set **1** reproduces the *t*-curve observed by the transient absorption measurements while the parameter set **2** cannot reproduce the *t*-curve. In parameter set **2**, RP dynamics slow down due to the expansion of the cage radius and the magnitude of the MFE does not reach the constant value even at the delay time of 3 μs. On the other hand, parameter set **3** can reproduce the *t*-curve observed by the transient absorption. However parameter set **3** can not reproduce the *B*-curve obtained at the delay time of 4 μs. Because of the low viscosity, the correlation times for the radicals and RP are shortened in parameter set **3**. The frequencies for molecular motions, which cause the spin relaxations, in parameter set **3** are higher than that in parameter set **1**. Thus the spin relaxations caused by the anisotropy of hyperfine interaction and the dipole-dipole interaction occur even in the presence of the higher magnetic field. As a result, the *B*-curve calculated with parameter set **3** is not saturated around 2 T, which differs from the *B*-curve observed by the transient absorption measurements. The present calculation with the three parameter sets suggests that fitting of both of *B*-curve and *t*-curve are necessary to extract the detailed information on the RP diffusion from the MFE data when the *B*-curve has no characteristic feature.

By fitting of the *B*-curve and the *t*-curve, we estimated the diffusion parameters (parameter set **1**) for the RP consisting of $XOH^{\bullet}$ and $XH^{\bullet}$ in the SDS micellar solution. The estimated parameters are in good agreement with the reported core radius and η values for the SDS micelle and are also consistent with the cage parameters obtained by the SLE analysis on the product-yield detected ESR observed for the photoreduction of anthraquinone in SDS micellar solution (D=$5.5\times10^{-11}m^2s^{-1}$ and P_{esc} = 5.2×10^{-4}).[28] The results show that one can extract the diffusion parameters in the nano-structured materials from simultaneous fitting of the *B*-curve and the *t*-curve of the MFE by using the SLE analysis proposed in the present study. Finally the *t*-curve obtained by method **1** is compared with that obtained by method **2**, which can correctly reproduce the oscillatory spin dynamics caused by the hyperfine interactions and Δg effect. Fig. 9 shows *t*-curve calculated by method **1** and method **2** with the parameter set **1**. The method **1** and **2** give the nearly identical results, indicating that method **1** can be applied to calculate the *t*-curve observed in the micellar solutions where the lifetime of RPs are longer than a few hundred nanoseconds.

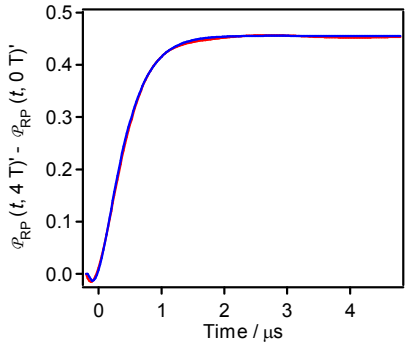

Fig. 9 Time evolution of magnetic field effect on the yield of radical calculated by method **1** (red line, identical with the red line in figure 8) and method **2** (blue line) with parameter set **1**. Method **1** gives the almost identical results with Method **2**. The data was obtained by subtracting the time profile of RP populations ($\Phi_{RP}(t)$) in the absence of the magnetic field from that obtained in the presence of the magnetic field of 4 T.

Conclusions

To calculate the *t*-curve of the MFE, we have developed the new method to solve the SLE by using the Miller-Guy procedure for the inverse Laplace transformation process. One can correctly calculate the time evolution of the MFEs in a short time by using our method when the spin coherence motions caused by the hyperfine interaction and the Δg effects are not important for the generation of the MFE. The *t*-curve and the *B*-curve of the MFE observed in micellar solution were simultaneously fitted by using the SLE. Our study demonstrated that simultaneous fitting of the *t*-curve and the *B*-curve of the MFEs provides the detailed information on the diffusion motion of the radical pair in nano-structured materials.

Acknowledgements

This work is supported in part by Grant-in-Aid for Young Scientist (B) (No. 25870123) and Grant-in-Aid for Scientific Research on Innovative Area of "All Nippon Artificial Photosynthesis for Living Earth" (Area No. 2406) (No. 25107509) from the Ministry of Education, Culture, Sports, Science and Technology (MEXT) of Japan.

Notes and references

[a] Department of Chemistry, Graduate School of Science and Engineering, Saitama University, 255 Shimo-ohkubo, Sakura-ku, Saitama, 338-8570, Japan.
e-mail: yago@chem.saitama-u.ac.jp

† Electronic Supplementary Information (ESI) available: Details of stochastic Liouville equation and parameters used in calculations. See DOI: 10.1039/b000000x/

1 U. E. Steiner and T. Ulrich, *Chem. Rev.*, 1989, **89**, 51–147.
2 H. Hayashi, *Introduction to Dynamic Spin Chemistry: Magnetic Field Effects upon Chemical and Biochemical Reactions*, World Scientific Pub Co Inc, Singapore, 2004.
3 C. T. Rodgers, *Pure Appl. Chem.*, 2009, **81**, 19–43.

4 Z. Schulten and K. Schulten, *J. Chem. Phys.*, 1977, **66**, 4616.
5 E. B. Krissinel, A. I. Burshtein, N. N. Lukzen, and U. E. Steiner, *Mol. Phys.*, 1999, **96**, 1083–1097.
6 A. Hamasaki, T. Yago, and M. Wakasa, *J. Phys. Chem. B*, 2008, **112**, 14185–14192.
7 K. Maeda, A. J. Robinson, K. B. Henbest, E. J. Dell, and C. R. Timmel, *J. Am. Chem. Soc.*, 2010, **132**, 1466–7.
8 N. J. Turro, B. Kraeutler, and D. R. Anderson, *J. Am. Chem. Soc.*, 1979, **101**, 7435–7437.
9 Y. Sakaguchi, S. Nagakura, and H. Hayashi, *Chem. Phys. Lett.*, 1980, **72**, 420–423.
10 J. C. Scaiano, E. B. Abuin, and L. C. Stewart, *J. Am. Chem. Soc.*, 1982, **104**, 5673–5679.
11 M. Okazaki, Y. Konishi, and K. Toriyama, *Chem. Phys. Lett.*, 2000, **328**, 251–256.
12 T. Maeyama, H. Matsui, T. Yago, and M. Wakasa, *J. Phys. Chem. C*, 2010, **114**, 22190–22196.
13 M. Wakasa, *J. Phys. Chem. B*, 2007, **111**, 9434–9436.
14 A. Hamasaki, T. Yago, T. Takamasu, G. Kido, and M. Wakasa, *J. Phys. Chem. B*, 2008, **112**, 3375–3379.
15 M. Wakasa, T. Yago, and A. Hamasaki, *J. Phys. Chem. B*, 2009, **113**, 10559–10561.
16 T. Yago and M. Wakasa, *J. Phys. Chem. C*, 2011, **115**, 2673–2678.
17 T. Yago, A. Hamasaki, M. Tanaka, T. Takamasu, and M. Wakasa, *J. Phys. Chem. C*, 2011, **115**, 21063–21071.
18 T. Okada, T. Yago, T. Takamasu, and M. Wakasa, *Phys. Chem. Chem. Phys.*, 2012, **14**, 3490–3497.
19 T. Yago, Y. Ishii, and M. Wakasa, *J. Phys. Chem. C*, 2014, **118**, 22356–22367.
20 R. Kubo, in *Advances in Chemical Physics: Stochastic Processes in Chemical Physics*, ed. K. E. Shuler, John Wiley & Sons, Inc., Hoboken, NJ, USA, 1969, vol. 15, pp. 101–127.
21 J. H. Freed, *Annu. Rev. Phys. Chem.*, 1972, **23**, 265–310.
22 J. B. Pedersen and J. H. Freed, *J. Chem. Phys.*, 1973, **58**, 2746–2761.
23 J. B. Pedersen and J. H. Freed, *J. Chem. Phys.*, 1973, **59**, 2869–2885.
24 J. H. Freed and J. B. Pedersen, in *Advances in Magnetic Resonance*, ed. J. S. Waugh, Academic Press, New York, 1976, vol. 8, pp. 1–84.
25 G. P. Zientara and J. H. Freed, *J. Chem. Phys.*, 1979, **70**, 2587.
26 F. J. J. Dekanter and R. Kaptein, *J. Am. Chem. Soc.*, 1982, **104**, 4759–4766.
27 V. F. Tarasov, N. D. Ghatlia, A. L. Buchachenko, and N. J. Turro, *J. Am. Chem. Soc.*, 1992, **114**, 9517–9526.
28 M. Okazaki and K. Toriyama, *J. Phys. Chem.*, 1995, **99**, 17244–17250.
29 Y. Kobori, K. Akiyama, and S. Tero-Kubota, *J. Chem. Phys.*, 2000, **113**, 465.
30 F. Ito, T. Ikoma, K. Akiyama, Y. Kobori, and S. Tero-Kubota, *J. Am. Chem. Soc.*, 2003, **125**, 4722–4723.
31 H. J. Werner, Z. Schulten, and K. Schulten, *J. Chem. Phys.*, 1977, **67**, 646–663.
32 K. Schulten and P. G. Wolynes, *J. Chem. Phys.*, 1978, **68**, 3292–3297.
33 H. Hayashi and S. Nagakura, *Bull. Chem. Soc. Jpn.*, 1984, **57**, 322–328.
34 M. K. Miller and W. T. Guy, Jr., *SIAM J. Numer. Anal.*, 1966, **3**, 624–635.
35 A. I. Shushin, *Chem. Phys. Lett.*, 1991, **183**, 321–326.
36 U. E. Steiner and J. Q. Wu, *Chem. Phys.*, 1992, **162**, 53–67.
37 I. A. Shkrob, *Chem. Phys. Lett.*, 1997, **264**, 417–423.
38 A. R. O'Dea, A. F. Curtis, N. J. B. Green, C. R. Timmel, and P. J. Hore, *J. Phys. Chem. A*, 2005, **109**, 869–73.
39 M. J. Hansen and J. B. Pedersen, *Riken Rev.*, 2002, **44**, 34–37.
40 C. P. Slichter, *Principles of Magnetic Resonance: with examples from solid state physics*, Harper & Row, New York, 1963.
41 G. Szegö, *Orthogonal Polynomials*, Ameircan Mathmatical Society, New York, 1939.
42 A. Erdélyi, Ed., *Tables of Integral Transforms Vol. 2*, McGraw-Hill, New York, 1954.
43 P. W. Atkins, *Physical Chemistry*, Oxford University Press, Oxford, 4th ed., 1990.
44 R. G. Mortimer, *Physical Chemistry*, Academic Press, San Diego, 2nd ed., 2000.
45 A. Schweiger and G. Jeschke, *Principles of Pulse Electron Paramagnetic Resonance*, Oxford University Press, New York, 2001.
46 K. Maeda, T. Miura, and T. Arai, *Mol. Phys.*, 2006, **104**, 1779–1788.
47 N. J. Turro, M. Grätzel, and A. M. Braun, *Angew. Chem. Int. Ed.*, 1980, **19**, 675–696.
48 J. K. Thomas, *Chem. Rev.*, 1980, **80**, 283–299.
49 N. J. Turro and B. Kraeutler, *Acc. Chem. Res.*, 1980, **13**, 369–377.
50 Y. Sakaguchi, H. Hayashi, and S. Nagakura, *J. Phys. Chem.*, 1982, **86**, 3177–3184.
51 C. Tanford, *J. Phys. Chem.*, 1972, **76**, 3020–3024.
52 N. C. Maiti, M. M. G. Krishna, P. J. Britto, and N. Periasamy, *J. Phys. Chem. B*, 1997, **101**, 11051–11060.
53 M. Graetzel and J. K. Thomas, *J. Am. Chem. Soc.*, 1973, **95**, 6885–6889.
54 J. Emert, C. Behrens, and M. Goldenberg, *J. Am. Chem. Soc.*, 1979, **101**, 771–772.
55 N. J. Turro, M. Aikawa, and A. Yekta, *J. Am. Chem. Soc.*, 1979, **101**, 772–774.
56 N. J. Turro and T. Okubo, *J. Am. Chem. Soc.*, 1981, **103**, 7224–7228.
57 W. D. Turley and H. W. Offen, *J. Phys. Chem.*, 1985, **89**, 2933–2937.